Droplet Impacting a Cantilever: A Leaf-Raindrop System

Sean Gart,[1] Joseph E. Mates,[2] Constantine M. Megaridis,[2] and Sunghwan Jung[1,*]
[1]*Department of Engineering Science and Mechanics, Virginia Tech, Blacksburg, Virginia 24060, USA*
[2]*Department of Mechanical and Industrial Engineering, University of Illinois at Chicago, Chicago, Illinois 60607, USA*
(Received 17 October 2014; revised manuscript received 12 March 2015; published 30 April 2015)

Previous studies show that air pollution and wind erosion, which damage a leaf's epicuticular wax layer, can change leaf surface properties from hydrophobic to hydrophilic. However, the dynamic response of a damaged leaf to a raindrop impact has not been investigated and could clarify the direct influence of changes in wettability on early leaf abscission. In this article, we investigate how leaves with different surface properties respond to falling raindrops, viewing this as a unique system of coupled elasticity and drop dynamics. An elastic beam with tunable surface wettability properties is used as a simple leaf model. We find that wettable beams experience much higher torque and bending energy than nonwettable beams. This is because a drop sticks to a wettable beam, while a drop falls off a nonwettable beam. An analytical model using momentum balance and simple cantilever beam theory quantifies the bending energy and torque experienced by wettable and nonwettable beams. The results elucidate the potential damage caused by raindrops impacting a leaf as a function of its surface wettability and are correlated with environmental factors contributing to premature changes of leaf surface properties.

DOI: 10.1103/PhysRevApplied.3.044019

I. INTRODUCTION

Leaf shedding is one of many survival mechanisms in deciduous plants to conserve water and nutrients during low-sun, dry, and cold winters [1,2]. The abscission process starts with the formation of a thin layer of dried dead cells at the base of the leaf stem and a change in surface property to hydrophilic [3,4]. Eventually, the leaf is separated from the stalk in response to torque induced by wind or rain. For example, oak tree leaves are hydrophobic when young but become hydrophilic due to wax-layer erosion before the end of the growing season [5]. The abscission mechanism is inadvertently triggered prematurely in areas with high levels of air pollution, accelerating forest decline [6–10]. Previous studies on this topic have focused on chemical reactions and associated wax-layer degradation [9,11,12]. However, the dynamic response of a contaminated leaf to high-speed drop impact may clarify the direct influence of air pollution on early leaf abscission, which has yet to be understood.

Hydrophobicity of a leaf surface plays an important role in keeping the surface clean as droplets roll, collect, and remove contaminants [13,14]; this is known as the lotus effect [15]. Most previous studies featured gently rolling drops or rigid and immobile leaves; however, in nature, raindrops hit a leaf at high speeds exhibiting drastically different dynamics as seen in Fig. 1. To investigate leaf-drop dynamics, we simplify the natural system by modeling a leaf using an elastic cantilever beam [16]. Droplet impact dynamics on rigid surfaces has been extensively studied [17–21], yet droplet impact on an elastic surface has not received much attention. These impacts can be important for industrial applications like piezoelectric raindrop energy harvesters [22–24] and can have biological implications like raindrops impacting leaves [25,26]. Though limited, there are several previous studies of droplet impact on elastic surfaces, such as the impact on a circular membrane [27], droplets bouncing on a soap film [28], and on the force of impacting rain [29]. Droplet impact on soft polydimethylsiloxane (PDMS) surfaces has also been studied [30,31], but there are no studies on how hydrophobic elastic surfaces respond to droplet impacts.

In this article, we investigate coupled cantilever beam and drop dynamics inspired by large raindrops impacting a leaf orthogonally near its free end (worst-case scenario in terms of potential for physical damage). The high-speed dynamics of droplet impact are recorded, while the bending energy ($\mathcal{E}$), torque ($\mathcal{T}$), vibration frequency (ω),

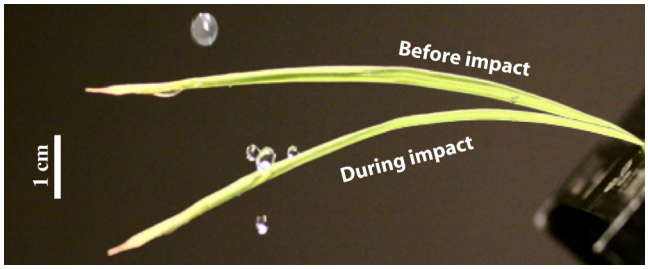

FIG. 1. Side view of water-drop impact on a natural leaf in the lab.

*sunnyjsh@vt.edu

and damping ratio (ζ) of the system are measured, and a simple theoretical model is developed to explain these measurements. The results of this study can be used to understand how leaf surface wettability affects the bending energy and torque on the leaf during raindrop impact, which can cause damage and contribute to early leaf fall.

II. METHODS AND MATERIALS

Our experimental apparatus has two parts: a drop dispenser and a polycarbonate cantilever beam [Fig. 2(a)]. Water is supplied very slowly using a syringe pump and exits through a flat-tipped capillary tube producing drops of radius ($R = 1.73 \pm 0.04$ mm) released from a height of 20 to 1300 mm, resulting in impact speeds (V) in the range 0.5 to 4.7 m/s. The drop radius used here is at the high end of typical raindrop sizes [32,33] and, thus, represents the worst-case scenario in terms of impact force, which scales with drop mass.

Water with surface tension $\sigma = 7.2 \times 10^{-2}$ N/m is used, and a drop release height of 100 mm used for most trials produces an impact speed of about 1.3 m/s. These values give Weber numbers ($\mathrm{We} = \rho V^2 D/\sigma$) of $O(10\text{–}1100)$, where ρ denotes fluid density and D drop diameter. Beam length (L) ranges from 50 to 160 mm, which is characteristic of many leaves. High-speed imaging is used to visualize droplet impacts on the beam. The elastic cantilever beam made of polycarbonate is clamped on one end, with the impact surface set at a zero angle with respect to the horizontal. The drops impact 5 mm from the beam free tip to avoid edge spilling during impact. This configuration represents another worst-case scenario for a leaf, as torque and bending energy depend on beam length and are maximized towards the free end of the beam.

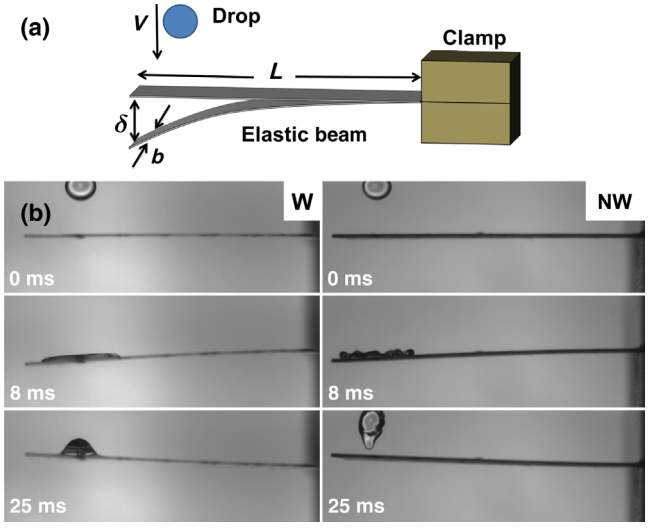

FIG. 2. (a) Schematic of the experiment setup. V denotes droplet impact velocity, δ the instantaneous beam-tip deflection, and L and b the beam length and width, respectively. (b) Temporally captured frames during impact of a water drop on W, an 80-mm-long wettable beam and NW, an 80-mm nonwettable beam.

Ambient air currents are minimized to reduce the deviation of impact location. For the 100-mm drop release height used in most trials ($V_{\mathrm{impact}} = 1.31 \pm 0.04$ m/s), the impact location from the beam end varies 5.0 ± 0.323 mm; however, for a drop height of 1300 mm ($V_{\mathrm{impact}} = 4.74 \pm 0.004$), the impact location has a greater variance (5.0 ± 3.23 mm). The maximum spreading diameter of the drop is 8.74 ± 0.79 mm at an impact speed of 1.31 m/s. For 7.75-mm-wide beams, the spreading diameter is slightly larger than the beam width, but no apparent spillage is observed from the recorded images. Spillage or splash and droplet fragmentation occur only at high impact speeds ($V_{\mathrm{impact}} = 4.74$ m/s). Beams are oriented such that the droplet always impacts orthogonally on the horizontal beam surface.

The wettability of the beams is changed using several different surface treatments. One group of beams tested has no surface treatment (i.e., polycarbonate surface), giving sessile contact angles (θ^*) of 71.7°; another group is coated with WX-2100 hydrophobic coating from Cytonix Co. giving $\theta^* \sim 153°$. Beams with $\theta^* = 82.0°$ and 57.7° are prepared via a spray-cast approach [34,35] (Paasche VL siphon feed, 0.55-mm nozzle); coatings are composed of all poly(methyl methacrylate) (PMMA) and a 40:60 blend of SiO_2:PMMA, respectively. (SiO_2 nanoparticles, 5–15 nm, and PMMA powder, solution processed in acetone, are both obtained from Sigma-Aldrich.)

Sessile contact angles θ^* are used to label the surfaces tested and are commonly employed to denote surface affinity to liquids but form an incomplete description of liquid wetting behavior and droplet mobility [36]. Advancing (θ_A^*) and receding (θ_R^*) contact angles are also measured to better understand droplet bouncing (hydrophobic) and adhesion (hydrophilic). An in-house goniometer is used to measure the advancing angles via a syringe-dispensed water droplet (approximately 10 μl); receding angles are measured as the liquid is withdrawn via the same method.

When discussing surface wetting, increased surface roughness is known to amplify the intrinsic wetting behavior of any surface [37]. For example, a high-energy surface becomes more hydrophilic when texture is added. A low-energy surface becomes more hydrophobic when textured. The advancing, receding, and sessile contact angles for the untreated and coated beams are reported in Table I; example images of the measurement procedure

TABLE I. Advancing (θ_A^*), receding (θ_R^*), and sessile (θ^*) contact angles for all polycarbonate beams tested (treated and untreated).

	θ_A^* (deg)	θ_R^* (deg)	θ^* (deg)
PMMA:SiO_2	75.0 ± 1.7	0.0 ± 0.0	57.7 ± 2.5
Untreated	91.3 ± 3.8	49.0 ± 2.6	71.7 ± 7.5
PMMA	91.0 ± 2.6	0.0 ± 0.0	82.0 ± 1.7
WX-2100	154.3 ± 2.1	150.0 ± 2.0	153.0 ± 3.0

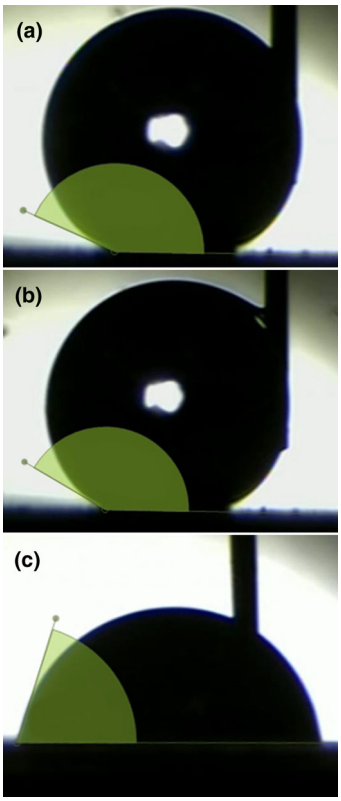

FIG. 3. (a) Advancing contact angle θ_A^* measurement on the WX-2100 treated surface. (b) Receding contact angle θ_R^* measurement for the same surface. The small contact angle hysteresis or difference between the advancing and receding angles translates to a low adhesive force. (c) θ_A^* for the PMMA : SiO_2-coated surface (θ_A^* is typically higher than θ^* since the liquid is not at equilibrium). The large hysteresis for this surface corresponds to a high adhesive force causing droplets to "stick."

are included in Fig. 3. With the exception of the untreated polycarbonate beams, the beams with $\theta^* < 82°$ have receding contact angles of 0° due to surface morphologies causing pinning of the droplet contact line. The untreated polycarbonate beams are observed to possess an inherent receding angle of approximately 49°, attributed to the smooth untextured polycarbonate surface. For the remainder of this paper, W will refer to beams on which the droplets stick, while NW will refer to beams on which the droplets bounce and fall off.

For wettable elastic beams ($\theta^* < 90°$), the drops impact, spread, and stick to the beam; see left column of Fig. 2(b). But for nonwettable beams ($\theta^* = 153°$), the drops impact, spread, and then fall off or bounce off the beam; see right column of Fig. 2(b). The beam continues to vibrate until damping is complete. Beam flexural rigidity (EI) values are $(2.96, 5.92, 11.61) \times 10^{-5}$ N m^2 for beams with width (b) of 7.75, 15.5, and 30.4 mm, respectively, and thickness (t) of 0.25 mm, where E is the elastic modulus and I is the cross-sectional inertia $I = bt^3/12$. The EI values are determined for all beams by placing a known weight on the tip of the beam and measuring tip deflection. Cross-species measurement of leaf petiole flexural rigidity has been shown to vary with length from 10^{-5} to 10^2 N m^2 [16], so our cantilever beams lie at the low end of natural petiole flexural rigidity.

III. EXPERIMENTAL RESULTS

Figure 4(a) plots the beam-tip position versus time for $\theta^* = 72°$ (W) and $\theta^* = 153°$ (NW) beams with lengths of 80 and 140 mm (15.5 mm width). For wettable beams, impacting droplets are observed to stick, which is consistent with the corresponding low receding contact angles θ_R^*; see Table I. As beam length increases, the mean downward deflection of the tip over time also increases. The nonwetting beams ($\theta^* = 153°$) oscillate about zero deflection, because droplets do not stick (consistent with the high receding contact angle θ_R^*; see Table I).

Wetting and nonwetting trends can be explained using a simple second-order differential equation of the form

$$\ddot{\delta}(t) + 2\zeta\omega_0\dot{\delta}(t) + \omega_0^2\delta(t) = 0, \tag{1}$$

where $\delta(t)$ is the tip deflection of the beam, ζ the damping ratio, and ω_0 the vibration frequency. Each of these terms, as well as a solution for $\delta(t)$ are discussed in the following paragraphs.

A. Beam vibration

Vibration frequency (ω_0) of each beam is calculated by averaging the time between peaks in the displacement data. All beams show good agreement with the first-mode theoretical vibration frequency [38]

$$\omega_0 = \beta^2\sqrt{\frac{EI}{m_{\text{beam}}L + m_{\text{drop}}}}\frac{1}{L^{3/2}}, \tag{2}$$

where m_{beam} is the beam mass per unit length and β a prefactor (for first-mode bending $\beta = 1.875$). Vibration frequency versus beam length is shown in Fig. 4(b).

The vibration frequencies of ten oak leaves (five in the spring growth season and five in the fall) are measured to compare with the current elastic beams. Leaves are collected and tested by clamping them at the end of their stem and perturbing them with a brief blow. The five leaves vary in length from 120 to 260 mm, but vibration frequencies for spring and fall leaves, respectively, are 17.15 ± 3.02 rad/s and 31.2 ± 7.92 rad/s corresponding to frequencies of elastic beams between 90 and 160 mm in length.

Figure 4(c) shows the theoretical damping ratio (dashed line) along with the damping ratio determined from the experiments by measuring the logarithmic decay of the tip motion. A cantilever beam has several sources of damping [39]: thermal, clamp, and air damping. Thermal elastic damping (TED) is defined as

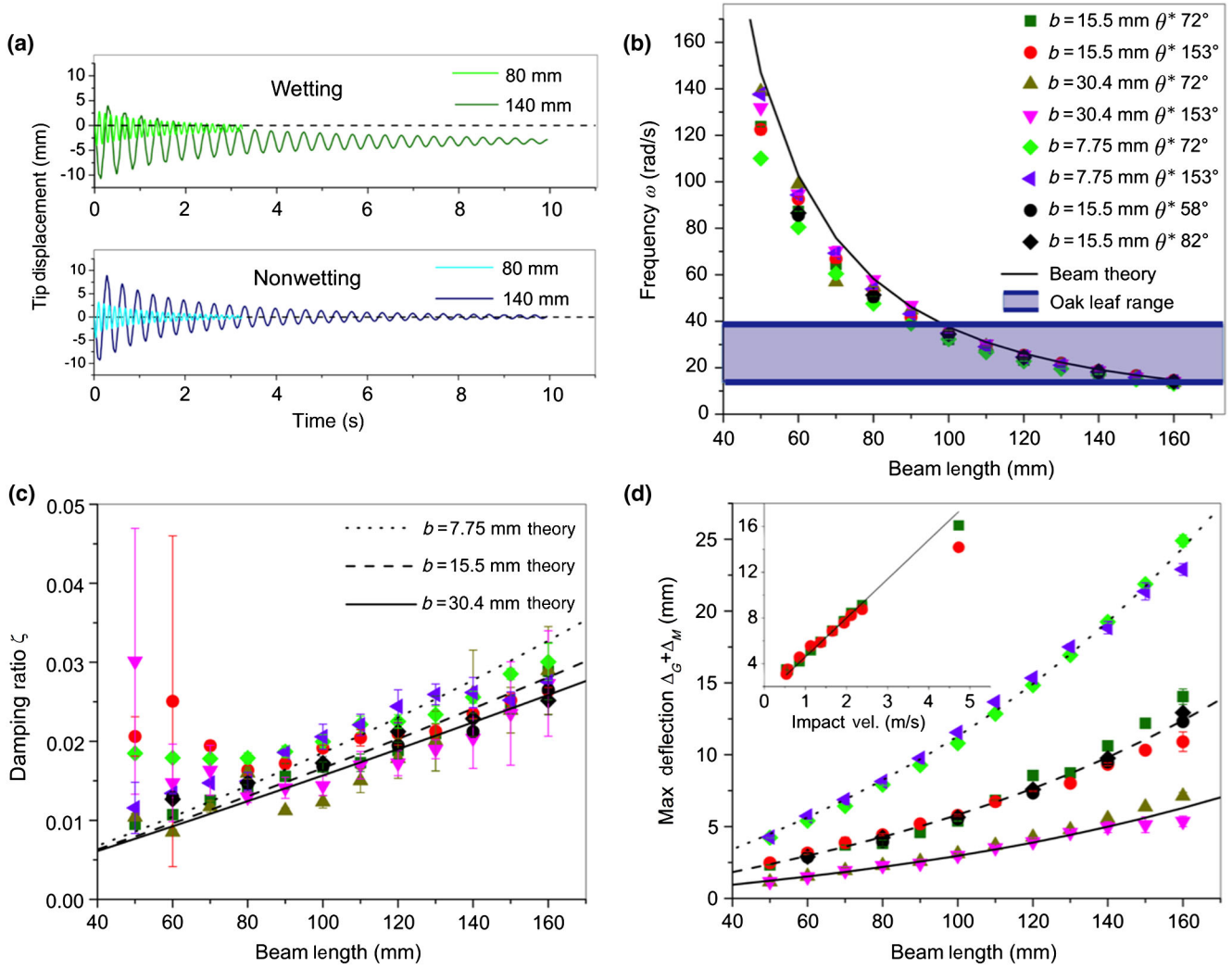

FIG. 4. (a) Beam-tip displacement versus time for 80- and 140-mm-long beams with $b = 15.5$ mm. The dashed line shows zero deflection. (b) Vibration frequency versus length for beams struck by a drop, and range of measured oak leaf frequencies. Theoretical first-mode frequency is also shown (beam theory). (c) Damping ratio versus beam length for beams struck by drops. The dashed and solid lines represent the theoretical ζ. (d) Maximum downward deflection versus beam length. The inset plots maximum deflection versus velocity for a 100-mm beam, and the dashed and solid lines represent $\Delta_M + \Delta_G$. All symbols correspond to the legend of Fig. 4(b).

$$\zeta_{\mathrm{TED}} = \frac{E\alpha^2 T_0 \omega_0 \tau_z}{[\rho_b C_p (1 + (\omega_0 \tau_z)^2]}, \tag{3}$$

where $\tau_z = \rho_b C_p t^2/(\pi^2 \kappa_{\mathrm{th}})$, ρ_b is the beam density, C_p the specific heat, α the linear thermal expansion coefficient, κ_{th} the thermal conductivity, and ω_0 the natural frequency of the beam. Damping from the beam support follows

$$\zeta_{\mathrm{clamp}} \propto (t/L)^3, \tag{4}$$

where t and L are the beam thickness and length, respectively.

For beams in this study, the air damping $O(10^{-2})$ is orders of magnitude higher than both thermal elastic damping $O(10^{-7})$ and clamp-support damping $O(10^{-5})$. To calculate the air-damping ratio, the air drag on the beam must be calculated first. This calculation can be done by approximating the beam as a series of oscillating spheres with radius $r = b/2$, where b is the beam width [40]. The drag on the spheres is found from Ref. [41], and the air-drag damping ratio is then

$$\zeta_{\mathrm{air}} = C_\zeta \frac{3\pi\mu b + \frac{3}{4}\pi b^2 \sqrt{2\rho_a \mu \omega_0}}{2\rho_b t b^2 \omega_0}, \tag{5}$$

where C_ζ is a prefactor (in this case, $C_\zeta = 3.8$), μ is the air viscosity, ρ_b is the beam density, and ρ_a the air density. C_ζ is found by fitting the experimental data with the previous expression. The damping ratio is determined from experiments by first calculating the logarithmic decay

$$\delta = \frac{1}{p}\ln\left[\frac{a(t_q)}{a(t_{q+pT})}\right], \tag{6}$$

where t_q is the qth peak, T the vibration period, p the number of cycles between peaks, and a the amplitude of vibration. The damping ratio is then

$$\zeta = \delta/\sqrt{4\pi^2+\delta^2}. \tag{7}$$

The predicted slope decreases as the beam width increases due to a decrease in air drag for the wider beams. Experiments show good agreement with the theory, although there is considerable overlap in the error bars. The damping ratio ζ weakly depends on the length of the beam, and its large variation for shorter nonwetting beams is due to the drops occasionally bouncing out of phase with the beam and quickly damping its vibration. The logarithmic decay method for calculating the experimental damping coefficient ζ is inconsistent when bouncing occurs.

B. Beam deflection

We can now find the solution for deflection, Eq. (1). For nonwettable beams, the drop bounces off of the beam, but for wettable beams, the drop sticks, meaning there is a constant downward Δ_G. Then, the solutions to the equation are

$$\delta_{\mathrm{NW}}(t) = (\Delta_M + \Delta_G)e^{-\zeta\omega_0 t}\cos(t\omega_0) \tag{8}$$

and

$$\delta_{\mathrm{W}}(t) = -\Delta_G + (\Delta_M + \Delta_G)e^{-\omega_0\zeta t}\cos(t\omega_0). \tag{9}$$

Δ_M is the deflection due to momentum transfer from the drop to the beam, and Δ_G is the deflection due to the weight of the droplet at the end of the beam. The momentum balance between a drop and the beam at an early stage [29] shows

$$m_{\mathrm{drop}}V = 4\Delta_M(m_{\mathrm{drop}} + m_{\mathrm{beam}}L/2)\frac{\omega_0}{2\pi}. \tag{10}$$

Then, by rearranging terms, we obtain

$$\Delta_M = \frac{\pi}{2}\frac{m_{\mathrm{drop}}}{m_{\mathrm{drop}} + m_{\mathrm{beam}}L/2}\frac{V}{\omega_0}, \tag{11}$$

where m_{drop} is the drop mass, m_{beam} the mass per unit length of the beam, and V the drop impact velocity. A simple torque balance delivers

$$\Delta_G = \frac{m_{\mathrm{drop}}gL^3}{3EI}. \tag{12}$$

On a wettable surface, the drop impacts the beam causing it to move downward due to the initial momentum transfer (Δ_M), but the drop does not fall off causing a constant $-\Delta_G$. For nonwetting beams, since the drop falls off, Δ_G must be included only in the initial deflection, as the drop does not fall off until after maximum deflection is reached.

Figure 4(d) shows initial maximum deflection ($\Delta_G + \Delta_M$) of the beam versus beam length; the inset shows initial maximum deflection versus impact velocity. There is very good agreement between the model (dashed line) and experiments. It can be seen that there is no obvious difference in maximum deflection between shorter, wettable, and nonwettable beams; at lengths over 120 mm, wettable beams seem to undergo a larger maximum deflection than nonwettable beams, although this difference is not significant.

C. Bending energy and torque

After characterizing frequency, damping, and amplitudes of oscillation, we now analyze bending energy and torque of the beams. Bending (or elastic) energy is the energy stored in a material while work is being done to deform it and can be converted to thermal or kinetic energy. For an object like a beam, the bending energy depends on the instantaneous curvature and rigidity of the beam. If there is too much deformation, then the bending energy is not conserved and the beam, or leaf stem, can be damaged. Measuring bending energy can also offer insight into how much electrical energy can be produced by a vibrating piezoelectric beam.

The average bending energy of an elastic beam is

$$\mathcal{E} \sim \frac{1}{(t_f - t_0)}\int_{t_0}^{t_f}\frac{EI}{2}\frac{\delta(t)^2}{L^3}dt. \tag{13}$$

For time integration, t_0 is set at the moment of drop impact, and t_f is the time required for the beam to undergo 25 vibration periods. In other words, $(t_f - t_0) = 2\pi N/\omega_0$, where N is 25. By inserting Eq. (8) into the bending energy Eq. (13), and if $t_f \gg t_0$, the expression for nonwetting bending energy becomes

$$\mathcal{E}_{\mathrm{NW}} = \frac{(\Delta_M + \Delta_G)^2(\zeta^2+1)EI}{8t_f\omega_0\zeta L^3}. \tag{14}$$

For wettable beams, there is additional force from the drop mass sticking to the end of the beam, and the expression for wetting displacement is seen in Eq. (9). If we insert Eq. (9) into Eq. (13), the bending energy expression becomes

$$\begin{aligned}\mathcal{E}_{\mathrm{W}} = {} & (\Delta_G)^2EI/(2L^3) - \Delta_M\Delta_G\zeta EI/(t_f\omega_0L^3) \\ & + (\Delta_M)^2(\zeta^2+1)EI/(8t_f\omega_0\zeta L^3).\end{aligned} \tag{15}$$

Four trials are run for each beam length, width, and impact velocity. If bending energy is multiplied by beam width b, and the damping ratio ζ, the data collapse, as

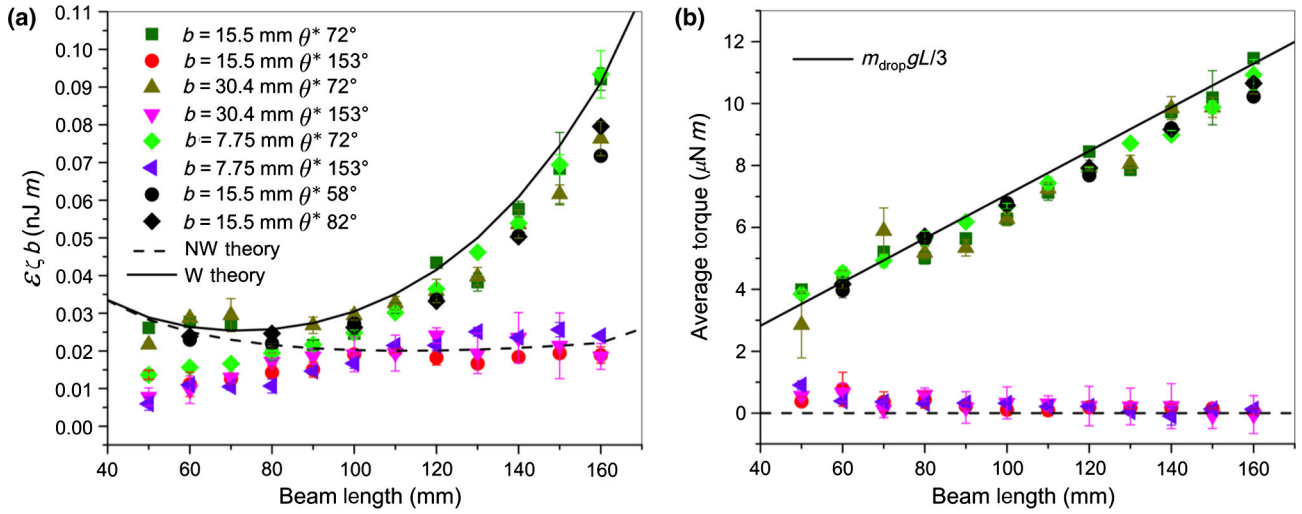

FIG. 5. (a) Measured beam bending energy multiplied by beam width b and damping ratio ζ. Theory from scaling arguments is shown with dashed (nonwetting) and solid (wetting) lines. (b) Torque versus beam length for wetting (W) and non-wetting (NW) beams. The dashed line shows zero torque, and the solid line shows the theoretical torque due to the droplet mass stuck to the beam.

shown in Fig. 5(a). Regardless of beam length and width, when the drop sticks, the wettable beam undergoes higher bending energy than when the drop rolls off the nonwettable beam. We also note that for nonwettable beams, droplets fall off the beam typically after a short time (approximately 160 ms) with the exception of the 50-mm-long beam where the drops do not fall off during some trials. For the 50-mm-long beams ($b = 15.5$ mm), drops tend to rebound at the same time the beam travels back upwards after its initial deflection. This deflection causes a "trampoline" effect in which the drop bounces straight up and down and sometimes does not fall off.

Equations (14) and (15) are multiplied by the beam width b and damping ratio ζ and plotted in Fig. 5(a) as "NW theory" and "W theory," respectively. The model agrees quite well with the experimental data for almost all beam lengths and widths. However, for (50–70)-mm-long nonwetting beams, the experiments indicate much less bending energy than the model predicts. This is due to the droplet bouncing on the end of the beam several times and quickly damping vibration.

A tree leaf experiences torque caused by bending stresses from external forces like wind and raindrop impacts. A higher torque on a leaf means it is more likely to fail. It has been shown that the highest bending stresses occur at the base of the petiole where the leaf connects to the stem [16], so we measure the torque at the beam base where it is clamped. The average torque at the base of the beam is measured similarly to the bending energy

$$\mathcal{T} \sim \frac{1}{(t_f - t_0)} \int_{t_0}^{t_f} EI \frac{\delta(t)}{L^2} dt. \tag{16}$$

The expressions for wetting and nonwetting displacement [Eqs. (8) and (9)] are then plugged into Eq. (16) to deduce the theoretical torque. For the nonwetting beams, Eq. (8) oscillates about zero; hence, the average torque becomes zero ($\mathcal{T}_{NW} \sim 0$). For the wettable case where the drop sticks, the torque $\mathcal{T}_W \sim m_{drop}gL/3$, which is consistent with simple cantilever beam theory. In Fig. 5(b), these trends are clearly observed. The ability of a beam to shed a drop significantly decreases the torque experienced by the beam over time and, hence, decreases potential damage from raindrop impact.

IV. DISCUSSION

The higher bending energy experienced by wettable beams suggests that a device intended to harvest energy from falling raindrops with a piezoelectric cantilever beam should be equipped with a hydrophilic surface. The added mass of a drop sticking to a beam increases deflection over time and causes the beam to store more elastic (bending) energy. This is verified using a 28-mm piezoelectric cantilever beam (LDT-028k from Measurement Specialties, Inc.). Impact velocity is varied, and a piezoelectric element with either a wetting or a nonwetting surface is used. One droplet impacting at the maximum speed produces about 23 nJ of electrical energy. Wettable piezoelectric cantilevers produce slightly greater electric energy, especially at higher velocities, as shown in Fig. 6.

Last, comparing the present bending energy and torque results to natural leaves is difficult due to the huge variation in leaf petiole stiffness and geometry found across plant species [16]. There have been limited studies on the breaking strength of a leaf petiole. One study reported a failure strength between 1.8 and 4.6 MPa for banana trees [42], which is similar to our simple tests showing failure strength between 1.5 and 3 MPa for tulip and ginkgo leaf petioles. The stress experienced by the beams in the present

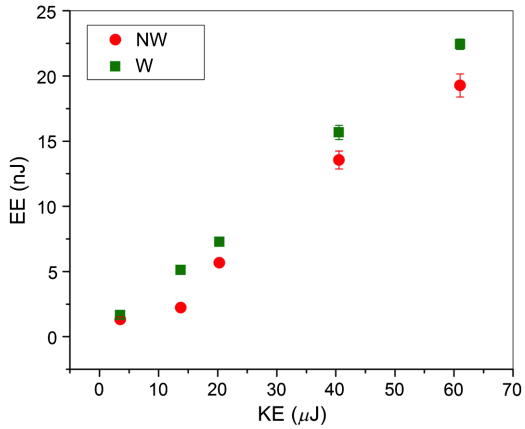

FIG. 6. Electrical energy (EE)—as captured by a piezoelectric cantilever with either a wettable (W) or non-wettable (NW) surface—versus drop impact kinetic energy (KE). EE is approximately one thousandth of the impact kinetic energy, a result of the energy conversion performed by the bending piezoelectric beam.

study from a single droplet impact is quite low (approximately 3.5 kPa) compared to the failure strength. Naturally, it will take many droplet impacts and vibration cycles to damage the leaf petiole; therefore, fatigue tests should be performed on actual leaves to clarify the effect of increased torque on leaf petioles due to droplet impact.

V. CONCLUSION

We perform large-droplet impact experiments on elastic cantilever beams with different surface treatments designed to modify wettability and measure the vibration frequency, damping ratio, initial deflection, torque, and bending energy. We compare these quantities to simple theoretical models. Elastic cantilevers are used as a simple model for a natural leaf in an attempt to elucidate whether or not leaves are protected from falling raindrops by virtue of their inherent surface properties.

We show that beams with a superhydrophobic ($\theta^* > 150°$) surface undergo zero average torque over time due to impacting drops bouncing and rolling off, while beams with a hydrophilic surface experience torque proportional to the drop weight and beam length due to sticking of the impacting drops. This outcome suggests that leaves with rain-repellent surfaces may be better protected from falling raindrops than leaves without repellent properties. When a drop impacts a beam and sticks, the beam vibrates with a mean downward displacement that is greater than when the drop is ejected. This causes a much higher torque experienced by hydrophilic beams, even though the initial beam deflection from the drop impact is roughly the same for both cases. These findings strengthen the case for premature erosion of the leaf's wax layer as a mechanism for early leaf abscission, likely a result of environmental factors such as wind erosion and air pollution.

ACKNOWLEDGMENTS

S. G. and S. J. acknowledge funding from the U.S. National Science Foundation (PoLS Grant No. 1205642). The authors also thank Daniel Chique, Josh Mull, and Dan Soto for useful discussions.

[1] R. Sexton and J. A. Roberts, Cell biology of abscission, Annu. Rev. Plant Physiol. **33**, 133 (1982).
[2] B. Rubinstein and A. C. Leopold, The nature of leaf abscission, Quart. Rev. Biol. **39**, 356 (1964).
[3] A. G. Gawadi and G. S. Avery, Jr., Leaf abscission and the so-called "abscission layer", Am. J. Bot. **37**, 172 (1950).
[4] C. Neinhuis and W. Barthlott, Seasonal changes of leaf surface contamination in beech, oak, and ginkgo in relation to micromorphology and wettability, New Phytol. **138**, 91 (1998).
[5] T. W. Brakke, W. P. Wergin, E. F. Erbe, and J. M. Harnden, Seasonal variation in the structure and red reflectance of leaves from yellow poplar, red oak, and red maple, Remote Sens. Environ. **43**, 115 (1993).
[6] F. Bussotti and M. Ferretti, Air pollution, forest condition and forest decline in Southern Europe: An overview, Environ. Pollut. **101**, 1 (1998).
[7] M. D. Thomas, Effects of air pollution on plants, Air Pollut. **46**, 233 (1961).
[8] M. Turunen and M. Huttunen, A review of the response of epicuticular wax of conifer needles to air pollution, J. Environ. Qual. **19**, 35 (1990).
[9] J. Burkhardt and S. Pariyar, Particulate pollutants are capable to "degrade" epicuticular waxes and to decrease the drought tolerance of Scots pine (Pinus sylvestris), Environ. Pollut. **184**, 659 (2014).
[10] G. H. Tomlinson, Air pollutants and forest decline, Environ. Sci. Technol. **17**, 246A (1983).
[11] E. A. Baker and G. M. Hunt, Erosion of waxes from leaf surfaces by simulated rain, New Phytol. **102**, 161 (1986).
[12] J. Wolfenden and T. A. Mansfield, Physiological disturbances in plants caused by air pollutants, Proc. R. Soc. Edinburgh B, **97**, 117 (1990).
[13] R. Blossey, Self-cleaning surfaces–virtual realities, Nat. Mater. **2**, 301 (2003).
[14] D. W. Bechert, M. Bruse, W. Hage, and R. Meyer, Fluid mechanics of biological surfaces and their technological application, Naturwissenschaften **87**, 157 (2000).
[15] W. Barthlott and C. Neinhuis, Purity of the sacred lotus, or escape from contamination in biological surfaces, Planta **202**, 1 (1997).
[16] K. J. Niklas, Research review: A mechanical perspective on foliage leaf form and function, New Phytol. **143**, 19 (1999).
[17] A. Yarin, Drop impact dynamics: Splashing, spreading, receding, bouncing …, Annu. Rev. Fluid Mech. **38**, 159 (2006).
[18] E. Villermaux, Fragmentation, Annu. Rev. Fluid Mech. **39**, 419 (2007).
[19] L. Xu, Liquid drop splashing on smooth, rough, and textured surfaces, Phys. Rev. E **75**, 056316 (2007).

[20] I. V. Roisman, E. Berberovic, and C. Tropea, Inertia dominated drop collisions. 1. On the universal flow in the lamella, Phys. Fluids **21**, 052103 (2009).
[21] J. Fukai, Y. Shiiba, T. Yamamoto, O. Miyatake, D. Poulikakos, C. M. Megaridis, and Z. Zhao, Wetting effects on the spreading of a liquid droplet colliding with a flat surface: Experiment and modeling, Phys. Fluids **7**, 236 (1995).
[22] R. Guigon, J. J. Chaillout, T. Jager, and G. Despesse, Harvesting raindrop energy: Theory, Smart Mater. Struct. **17**, 015039 (2008).
[23] R. Guigon, J. J. Chaillout, T. Jager, and G. Despesse, Harvesting raindrop energy: Experimental study, Smart Mater. Struc. **17**, 015038 (2008).
[24] P. V. Biswas *et al.*, in *Proceedings of the International Conference on Mechanical Engineering* (Bangladesh University of Engineering and Technology, Dhaka, Bangladesh, 2009).
[25] G. J. Amador, Y. Yamada, M. McCurley, and D. L. Hu, Splash-cup plants accelerate raindrops to disperse seeds, J. R. Soc. Interface **10**, 20120880 (2012).
[26] T. Gilet and L. Bourouiba, Rain-induced ejection of pathogens from leaves: Revisiting the hypothesis of splash-on-film using high-speed visualization, Integr. Comp. Biol. **54**, 974 (2014).
[27] R. E. Pepper, L. Courbin, and H. Stone, Splashing on elastic membranes: The importance of early-time dynamics, Phys. Fluids **20**, 082103 (2008).
[28] T. Gilet and J. W. M. Bush, The fluid trampoline: Droplets bouncing on a soap film, J. Fluid Mech. **625**, 167 (2009).
[29] D. Soto, A. B. De Larivière, X. Boutillon, C. Clanet, and D. Quéré, The force of impacting rain, Soft Matter **10**, 4929 (2014).
[30] S. Mangili, C. Antonini, M. Marengo, and A. Amirfazli, Understanding the drop impact phenomenon on soft PDMS substrates, Soft Matter **8**, 10045 (2012).
[31] R. Rioboo, M. Voué, H. Adão, J. Conti, A. Vaillant, D. Seveno, and J. De Coninck, Drop impact of soft surfaces: Beyond the static contact angles, Langmuir **26**, 4873 (2010).
[32] E. Villermaux and B. Bossa, Single-drop fragmentation determines size distribution of raindrops, Nat. Phys. **5**, 697 (2009).
[33] C. W. Ulbrich, A review of the differential reflectivity technique of measuring rainfall, IEEE Trans. Geosci. Remote Sens. **GE-24**, 955 (1986).
[34] J. E. Mates, T. M. Schutzius, I. S. Bayer, J. Qin, D. E. Waldroup, and C. M. Megaridis, Water-based superhydrophobic coatings for nonwoven and cellulosic substrates, Ind. Eng. Chem. Res., **53**, 222 (2014).
[35] J. E. Mates, T. M. Schutzius, J. Qin, D. E. Waldroup, and C. M. Megaridis, The fluid diode: Tunable unidirectional flow through porous substrates, ACS Appl. Mater. Interfaces, **6**, 12837 (2014).
[36] L. Gao and T. J. McCarthy, Contact angle hysteresis explained, Langmuir **22**, 6234 (2006).
[37] D. Quéré, Wetting and roughness, Annu. Rev. Mater. Res. **38**, 71 (2008).
[38] L. Meirovitch, *Fundamentals of Vibrations* (McGraw-Hill, New York, 2001), pp. 419–420.
[39] K. Naeli and O. Brand, Dimensional considerations in achieving large quality factors for resonant silicon cantilevers in air, J. Appl. Phys. **105**, 014908 (2009).
[40] H. Hosaka, K. Itao, and S. Kuroda, Damping characteristics of beam-shaped micro-oscillators, Sens. Actuators. A Phys. **49**, 87 (1995).
[41] L. D. Laundau and E. M. Lifshitz, *Fluid Mechanics* (Pergamon, London, 1959), p. 95.
[42] R. L. Chazdon, The costs of leaf support in understory palms: Economy versus safety, Am. Naturalists **127**, 9 (1986).